Tellus (1999), 51A, 663–673
Printed in UK – all rights reserved

TELLUS
ISSN 0280–6495

Convergence of atmospheric simulations with increasing horizontal resolution and fixed forcing scales

By DAVID L. WILLIAMSON, *National Center for Atmospheric Research*, Box 3000, Boulder, Colorado 80307-3000, USA*

(Manuscript received 14 September 1998; in final form 16 February 1999)

ABSTRACT

A series of experiments with the NCAR Community Climate Model, Version 2 (CCM2) is examined in which the grid and scale of the physical parameterizations are held fixed while the horizontal resolution of the dynamical core is increased. The convergence characteristics of these dual-resolution simulations are compared to those of simulations with the standard model in which the resolutions of both the dynamical core and physical parameterizations are increased together, as traditionally done in atmospheric model convergence studies. With the standard model the upward branch of the local Hadley circulation increases in strength with increasing horizontal resolution and does not converge by T170 truncation. As the dynamical resolution is increased, but the parameterization resolution held fixed, the dual-resolution model simulations converge to a state close to that produced by the standard model at the fixed parameterization resolution. The mid-latitude transient aspects do not converge with increasing resolution when the scale of the physics is held fixed. The nonlinear interactions in the dynamics create finer scales, with or without the finer scale forcing. However, the lower resolution T42 scales appear to converge. These convergence characteristics are shared by both the dual-resolution model and the standard model when horizontal resolution is increased.

1. Introduction

In many atmospheric general circulation models, when horizontal resolution is increased traditional large scale statistics of the mean climate seem to converge. This convergence occurs in the range of T42 to T63 truncation in spectral models (Boyle, 1993; Williamson et al., 1995). However, at least in some models, regional aspects of the climate do not converge in the resolution range commonly adopted in climate models today (Déqué et al., 1994; Déqué and Piedelievre, 1995; Sperber et al., 1994; Stephenson et al., 1998), nor do the processes that produce these climates (Williamson et al., 1995). These processes have been examined much less thoroughly than the statistics themselves. Fields such as the local, large scale pressure vertical velocity ω are sensitive to resolution and sub-grid scale parameterizations. For example, multi-year simulations with several versions of the NCAR CCM indicate that the upward branch of the local Hadley circulation continues to increase in strength with increasing horizontal resolution. It does not converge by T170 (T106) truncation with CCM2 (CCM1), the highest resolution considered with each version (Williamson et al., 1995; Kiehl and Williamson, 1991). Similarly, Stephenson and Royer (1995) and Stephenson et al. (1998) report intensification of the equatorial convergence zones with increasing horizontal resolution, and there are similar indications in Potter (1995) in the net cloud radiative forcing, although he does not specifically call them out. Although much of this non-conver-

e-mail: wmson@ncar.ucar.edu.
* The National Center for Atmospheric Research is sponsored by the National Science Foundation.

gence with increasing horizontal resolution is associated with the addition of finer scales which are not present at lower resolutions, we will see below that in some cases the coarser scale component does not converge.

The differences in ω described above are accompanied by differences in the forcing produced by the physical parameterizations. For example, as resolution increases in CCM2 condensation increases throughout the column of the ascending branch of the Hadley cell, where stronger ascending motion is producing more vertical transport by the resolved scales. This, of course, results in stronger heating from the release of latent heat which feeds back further on the upward motion. The parameterizations themselves seem to depend on resolution and work differently at higher resolution.

The characteristics of the processes in the mid-latitudes are harder to examine in a mean sense because the phenomena involved are not stationary. The translating synoptic systems preclude simple temporal averaging as a means of analysis. For example, upward and downward vertical motion cancel in a temporal average and provide little information on the average strength of the systems. Thus, the characteristics of ω in mid-latitudes have been examined to a lesser extent. However, calculations with CCM1 (Kiehl and Williamson, 1991) indicated significant changes in the probability density distribution of ω in the North Atlantic storm track region with increasing resolution up to T106. Stratton (1999) also found changes in the probability density distribution of ω over Northern Hemisphere mid-latitude land and to a lesser extent over oceans.

In many computational fluid dynamical applications, the scale of the forcing is held fixed as resolution is refined and a convergent solution is obtained. In atmospheric modeling, the sub-grid scale parameterizations are calculated for individual grid cells and often produce grid scale structures. Generally, the scale of the grid box is not explicitly accounted for in the parameterizations. Thus the scale of the forcing decreases with increasing horizontal resolution which may be leading to the lack of convergence. In the following we examine the convergence of a series of simulations in which the scale of the parameterizations is held fixed as horizontal resolution of the dynamics is increased. We compare the convergence characteristics of this series with those of the standard model where parameterizations and dynamics are based on the same scales.

2. Brief description of CCM2

Complete details of the algorithms of CCM2 are provided by Hack et al. (1993). Here, we simply list the components of the model. The dry dynamics are approximated with a horizontal spectral transform method and nominally second order vertical finite differences coupled with a semi-implicit, leapfrog time integration scheme. Water vapor transport is treated with a monotonic semi-Lagrangian scheme (Williamson and Rasch, 1994). Fourth order horizontal diffusion is applied to the dynamical variables but not to water vapor.

CCM2 contains a complete complement of physical parameterizations. The planetary boundary layer is parameterized by a nonlocal scheme (Holtslag and Boville, 1993). A simple mass flux scheme represents all types of moist convection (Hack, 1994). The diagnosed cloud fraction depends on relative humidity, vertical motion, static stability, and convective precipitation rate (Kiehl et al., 1994). The δ-Eddington solar radiative heating parameterization is described in Briegleb (1992). Both diurnal and annual cycles are included. The longwave radiation parameterization is described in Kiehl and Briegleb (1991). McFarlane's (1987) parameterization of momentum flux divergence by stationary gravity waves is included.

The land temperature is calculated for a soil with finite heat capacity, represented by a 4-layer diffusion model with heat capacities specified for each layer to capture the major observed climatological cycles. The land has specified soil hydrologic properties. Sea surface temperatures and sea ice distributions are specified by linear interpolation between the climatological monthly mean values of Shea et al. (1990). Sea ice temperatures are calculated like the land temperatures but with thermal properties appropriate for sea ice.

The standard model configuration is 18 vertical levels with an explicit lid at 3 mb, and T42 horizontal spectral truncation. Many of the papers cited above, which document various individual components of the model, also describe aspects of the simulated climate produced by this model configuration. In addition, basic climatological statistics from the standard 18 level, T42 simulation are discussed in Hack et al. (1994). The model's simulated earth radiation budget is documented in Kiehl et al. (1994). Williamson et al. (1995) describe simulations with the 18-level CCM2 at different horizontal resolutions, and present a variety of results from R15, T21, T31, T42, T63 and T106 horizontal truncations. A T170 simulation was completed after that paper was published. These simulations at various resolutions are used here for comparative purposes. This version of the model will be referred to as the *standard* model.

3. Dual-resolution CCM2

Some modifications were required in CCM2 in order to calculate the parameterizations at a different horizontal resolution than the dynamics. This version of the model will be referred to as the *dual-resolution* model.

In general, the prognostic equation for a generic model variable ψ can be written as

$$\frac{\partial \psi}{\partial t} = D(\psi) + T(\psi) + A(\psi), \tag{1}$$

where D represents the adiabatic dynamics. In (1), we have divided the parameterizations into two categories, T and A, depending on their treatment in the standard model. A represents those parameterizations applied in a time-split manner in the standard model. We refer to these as adjustment parameterizations since they adjust the state sequentially. T represents those physical parameterizations applied in a process-split manner in the standard model. We refer to these as tendency parameterizations since they result in a tendency or forcing applied to the dynamics.

In the standard model (1) is approximated by the following sequence.

$$\psi^* = \psi^{n-1} + 2\Delta t T(\psi^*, \psi^{n-1}), \tag{2}$$

$$\psi^{**} = \psi^{n-1} + 2\Delta t D(\psi^{**}, \psi^n, \psi^{n-1}) + 2\Delta t \left[\frac{\psi^* - \psi^{n-1}}{2\Delta t}\right], \tag{3}$$

$$\psi^{n-1} = A(\psi^{**}). \tag{4}$$

In the first step (2), the process-split, tendency parameterizations are calculated implicitly. The tendency or forcing from these parameterizations is retrieved after solving (2), and is applied as a forcing during the dynamics step (3). Note that the combination (2) and (3) does not represent a time-split approximation since D in (3) depends on ψ^{n-1} rather than ψ^* which would be the time-split case. The parameterizations in the third step (4) are then applied in a time-split manner to produce an adjustment of the state produced by the dynamics. This adjustment component consists of the large scale precipitation and convective parameterizations.

For the dual-resolution simulations, this sequence was replaced by the following in order to calculate the net effect of all the parameterizations in a time-split manner, but retain the particular ordering and dependencies of the parameterizations in the standard model.

$$\psi^* = \psi^{n-1} + 2\Delta t D(\psi^*, \psi^n, \psi^{n-1}), \tag{5}$$

$$\psi^{**} = A(\psi^*), \tag{6}$$

$$\psi^{***} = \psi^{**} + 2\Delta t T(\psi^{***}, \psi^{**}), \tag{7}$$

$$\psi^{n-1} = \psi^* + 2\Delta t \left[\frac{\psi^{***} - \psi^{**}}{2\Delta t} + \frac{\psi^{**} - \psi^*}{2\Delta t}\right]. \tag{8}$$

The dynamical component is advanced first without any forcing (5). The state produced by the dynamics is then modified by the adjustment parameterizations (6), and that adjusted state is used as the basis of the tendency parameterizations (7). Thus, we see that the sequence of the parameterizations is the same as in the standard model where the tendency parameterizations (2) work off the state produced by the adjustment parameterizations (4) and the adjustment parameterizations work off the state produced by the dynamics. Finally, the two sets of parameterizations are converted to rates and added to the state produced by the dynamics (8). When the parameterizations and dynamics are at the same resolution this last step (8) is not explicitly performed since $\psi^{n+1} = \psi^{***}$. It is formally included in the description here for the convenience of the case of different resolutions described in the next paragraph. Although the order of application of the various parameterizations is the same in the standard and the dual-resolution models, the state corresponding to a full time step is not in the same state of equilibrium in both, and the simulation statistics might appear to be different. However, when the parameterizations and dynamics were calculated at the same T42 resolution, the procedure (5)–(8) gave a simulation which was essentially the same as produced by the original (2)–(4) for the quantities considered in this paper.

In order to calculate the parameterizations and dynamics at different resolutions, the state produced by the dynamics in (5), ψ^*, is temporarily truncated in spectral space to the parameterization resolution and grid values are calculated from the truncated coefficients on the quadratic Gaussian grid consistent with that truncation. The water vapor specific humidity is bi-linearly interpolated to the same grid. After the parameterizations have been calculated on the parameterization grid, the implied forcing (term in square brackets in (8)) is expanded to spectral space at the parameterization truncation and added to the original untruncated coefficients of the state variables at the dynamics resolution. The state variables are then resynthesized on the higher resolution dynamics grid. The parameterization source and sink terms for the water vapor are bi-linearly interpolated to the high resolution dynamics grid and added to the specific humidity.

There is only one problem with this approach as described. After five or six months of integration the model blew up. This was traced to the nonlinear surface exchange. In certain circumstances, when calculated only on the coarse grid, the surface stress, which should damp, amplified small scale local structures not seen by the coarse resolution stress. This rapidly lead to the blow up. The dual-resolution model was stabilized by applying a linear stress to all scales first and then removing it from the larger parameterization scales. That is, a linear version of the stress was included in (5) at the dynamics resolution in the manner of the tendency parameterizations in (2) and (3) of the standard model. This linear stress was truncated to the parameterization resolution along with the predicted state variables, and subtracted from the forcing on the coarse grid (7) where the nonlinear stress was calculated. Thus the model saw the nonlinear stress on the parameterization resolution component and the linear stress on the additional smaller scales included in the dynamics.

In the dual-resolution model, all parameterization coefficients were set to the values normally used in the standard model when run at the physics resolution, except the horizontal diffusion, which we associate with the dynamics. The diffusion coefficients were set to be those used by the standard model when run at the dynamics resolution. Those values are given in Williamson et al. (1995). The surface orography in the dual-resolution simulations, which explicitly enters the dynamics but not the parameterizations, was set to that used by the standard model when run at the dynamics resolution.

Simulations were made with parameterizations at T31 truncation coupled with dynamics at T63 and T106, and with parameterizations at T42 also coupled with dynamics at T63 and T106. We concentrate on the T42 parameterization simulations here. Results from the T31 parameterization simulations are similar. The dual-resolution model simulations all started 1 September from a simulation by the standard model and ran through the fourth January. The analyses were calculated over the four simulated Januaries, or the three simulated Julies.

4. Tropical mean circulation

Fig. 1 shows meridional cross sections of multi-year January averaged, zonal average pressure vertical velocity ω for the Atlantic basin, averaged from 30°W to 7.5°E. The first row shows ω from the standard model at horizontal spectral truncations of T42, T63 and T106. (The simulations and number of Januaries averaged are described in Williamson et al., 1995.) The most conspicuous signal is the increase in strength and depth of the upward cell ($\omega < 0$) with increasing resolution. Both the depth and strength increase even more in the T170 simulation (not shown). The right panel in the first row shows ω from the T106 simulation truncated to T42 and plotted on the T42 grid (denoted T106@T42). The increased strength and depth are present in the larger scale T42 component of the higher resolution simulation. The T42 component of the T170 simulation is even stronger and deeper. The second row shows ω from the dual-resolution simulations with the parameterization resolution at T42 and the dynamics at T63 and T106, denoted T63/T42 and T106/T42, respectively. Values are shown on the

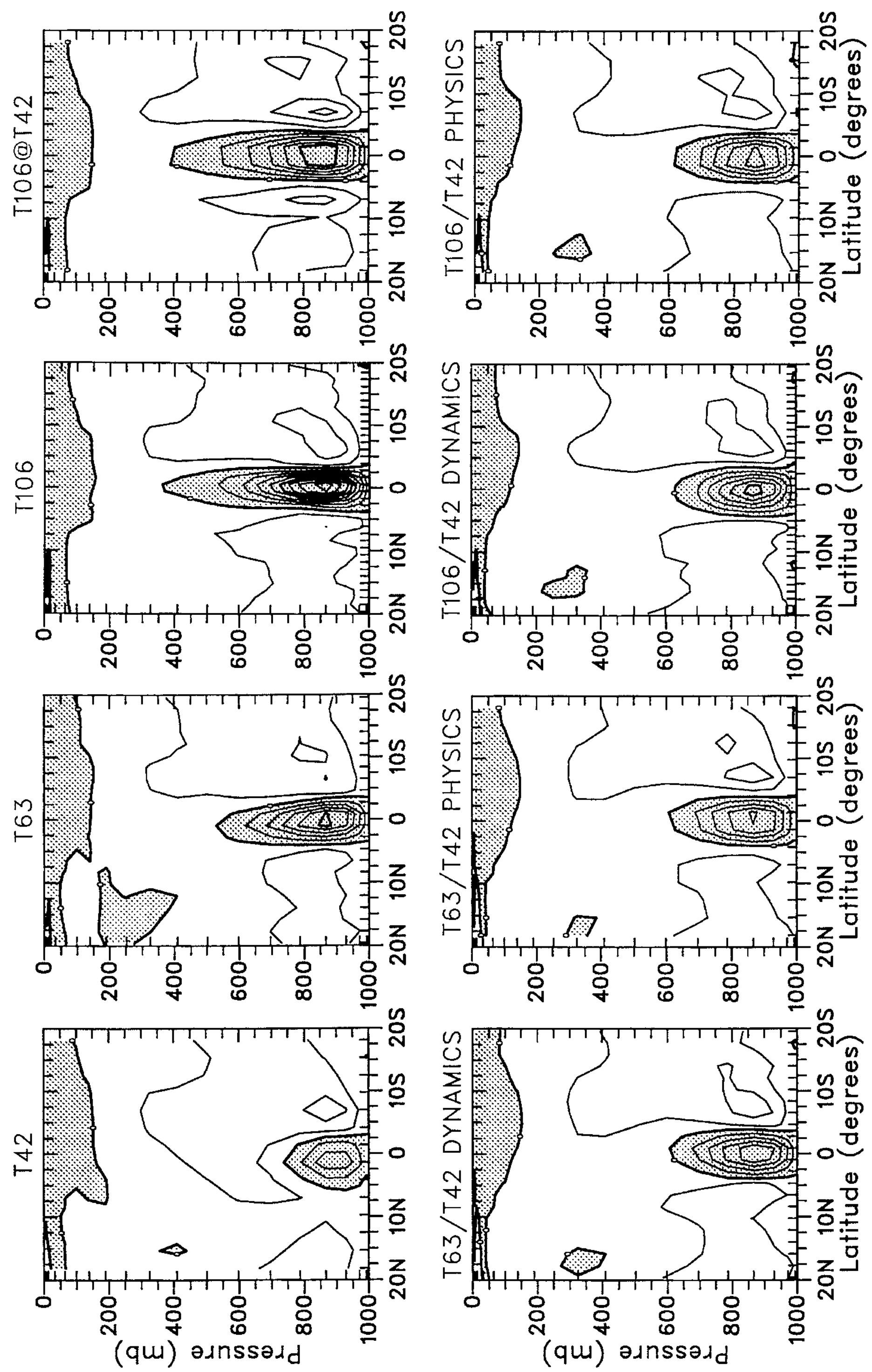

Fig. 1. January average, zonal average over Atlantic basin (30°W to 7.5°E) pressure vertical velocity (ω). Contour interval is 20 mb day^{-1}, negative (upward) regions stippled.

dynamics grid, labeled DYNAMICS, and on the parameterization grid, labeled PHYSICS. Values from the same simulation are very similar on the two grids. When looked at on the finer dynamics grid, both dual-resolution cases fall between the standard T42 and T63 cases. The T63/T42 upward cell is not as deep as the standard T63 and the T106/T42 cell has strength similar to standard T63 but is not as deep. However, the difference between the T63/T42 and T106/T42 is in the extra dynamical scales. On the T42 parameterization grid the simulations have converged to a state close to that produced by the standard model at a resolution close to that supported by the parameterization grid, i.e. T63. Recall that waves up to T63 are representable on the T42 quadratic grid used for the parameterization, and ω is diagnosed from a nonlinear combination of the T42-truncated state variables.

The upward cells in the dual-resolution T63/T31 and T106/T31 simulations (not shown) have similar characteristics to those described above. The T106/T31 resembles the standard T42 more than the T31, although the T63/T31 is closer to the standard T31. Other periods and regions also show similar behavior for both the T31-based and T42-based dual-resolution models. For example, the July averaged ω in the equatorial eastern Pacific, averaged from 180°W to 105°W has a variation similar to that in Fig. 1, however the January average for that region shows a weaker, although still noticeable, signal.

Fig. 2 shows the zonal average specific humidity tendency from the stable condensation and convective parameterizations in the equatorial Atlantic. The T42 standard model simulation shows detrainment from the convective parameterization above 800 mb throughout much of the tropical Atlantic region including weak detrainment in the upward branch of the Hadley circulation. The T63 and T106 simulations show the detrainment associated with the trade cumulus on the subsiding flanks of the Hadley cell, but they also show condensation throughout the column of the ascending branch, where stronger ascending motion is producing more vertical transport by the resolved scales. The strength and depth of the condensation increases from T63 to T106, in concert with the vertical motion in Fig. 1. The physical mechanisms affecting the vertical distribution of water vapor are acting very differently at the different resolutions. Fig. 2 also shows the specific humidity tendency from the dual-resolution T63/T42 and T106/T42 simulations on the T42 parameterization grid where it was calculated. Again, the characteristics of the distribution fall between the T42 and T63 of the standard model, both in strength and depth, and the T63/T42 and T106/T42 fields are virtually the same. This aspect of the simulation has also converged.

5. Northern hemisphere transient circulation

Fig. 3A shows the January probability density distribution of daily averaged values of ω at 850 mb in the North Atlantic storm track region (30°N to 60°N, 60°W to 30°W) for simulations from the standard model run at T42 and T106 spectral truncations. There is a distinct shift in skewness toward subsidence with increasing resolution. In addition, the probability of stronger upward motion increases with higher resolution, and that of weaker upward motion decreases. The shift in the distribution from T42 to T106, particularly the increased frequency of upward motions stronger than 250 mb/day, is due to the additional finer scales included in the T106 simulation. This is seen in Fig. 3B which shows the distribution of the T106 simulated daily averaged ω truncated to T42 (denoted T106@T42) compared to the full T106 data. The figure looks very much like Fig. 3A indicating that the difference with increasing resolution is in the additional smaller scales. The simulations do not converge with increasing resolution, but the T42 component does converge and is not strongly affected by the additional scales.

Fig. 3C shows the distribution of ω from the T106 dynamical component of the dual-resolution T106/T42 simulation (labeled DYNAMICS) compared to the T106 standard model distribution. Fig. 3D shows the distribution from the T42 parameterization component of the dual-resolution T106/T42 simulation (labeled PHYSICS) compared to the T42 standard model distribution. The T106 dynamical component in the dual-resolution model captures much of the T106 standard model simulation signal. The smaller scales in ω are not directly forced by the finer resolution parameterizations, but rather result from nonlinear inter-

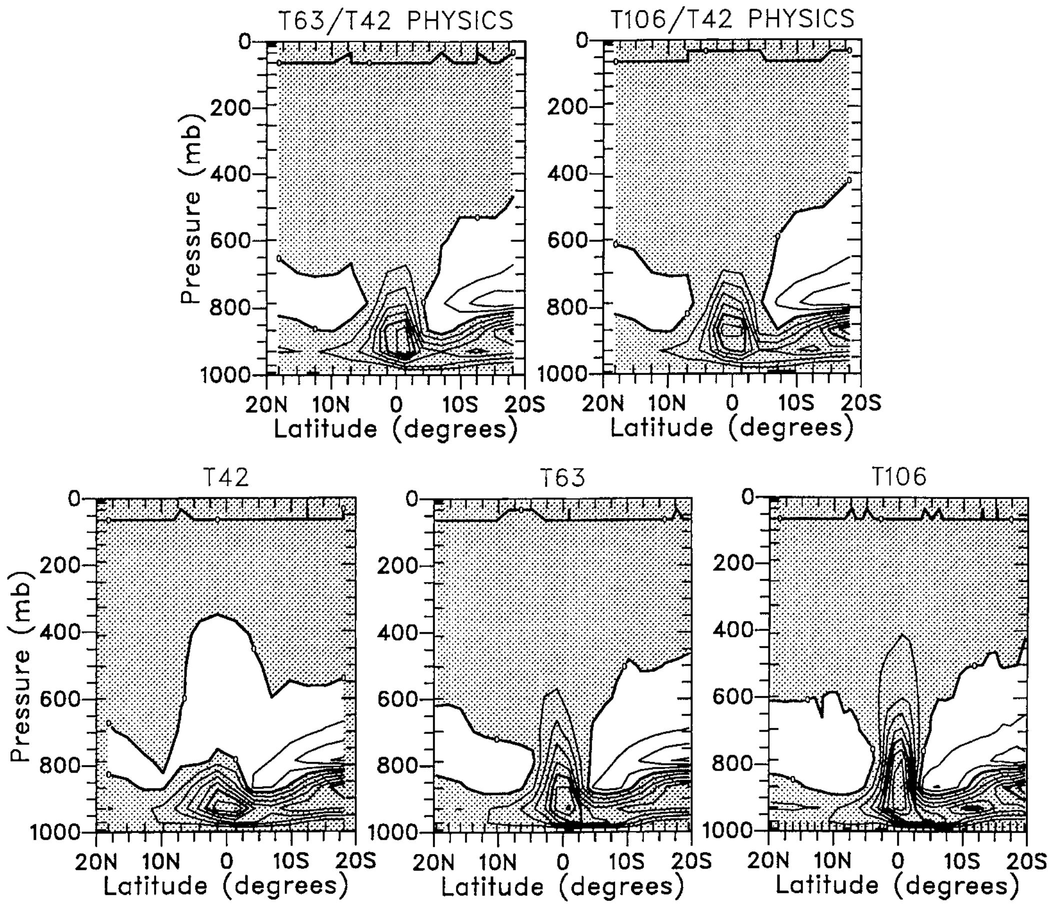

Fig. 2. January average, zonal average over Atlantic (30°W to 7.5°E) specific humidity tendency due to convective parameterization and stable condensation. Contour interval is 0.5 g kg^{-1} day^{-1}, negative (detrainment) regions stippled.

actions in the dynamics. The truncated T42 component of the dual-resolution T106/T42 model seen by the parameterizations is closer to that of the standard T42 simulation, consistent with the standard T106 model ω truncated to T42 shown in Fig. 2B.

As mentioned in Section 3, the surface orography in the dual-resolution simulations has the resolution of the dynamical component. In the standard model, the ringing in the orography becomes noticeably worse going to higher resolution, in part simply because the truncation scale becomes more separated from the large physical scales of the major mountain ranges and the noise becomes more visually obvious on inspection. Likewise, the vertical motions induced by that noise become more obvious at higher resolution because the truncation scale becomes more separated from the synoptic scales. It is conceivable that the resolution signal in the probability density distribution of ω discussed in the previous section is affected by that temporal mean signal. We have calculated the probability density distribution from the January monthly means and that is not the case. All the power is confined in the categories close to zero for the density distribution calculated from the monthly means. The density distributions calculated from the eddies match those from the total field shown in Fig. 3. Thus the signal discussed above is associated with the eddies, and pre-

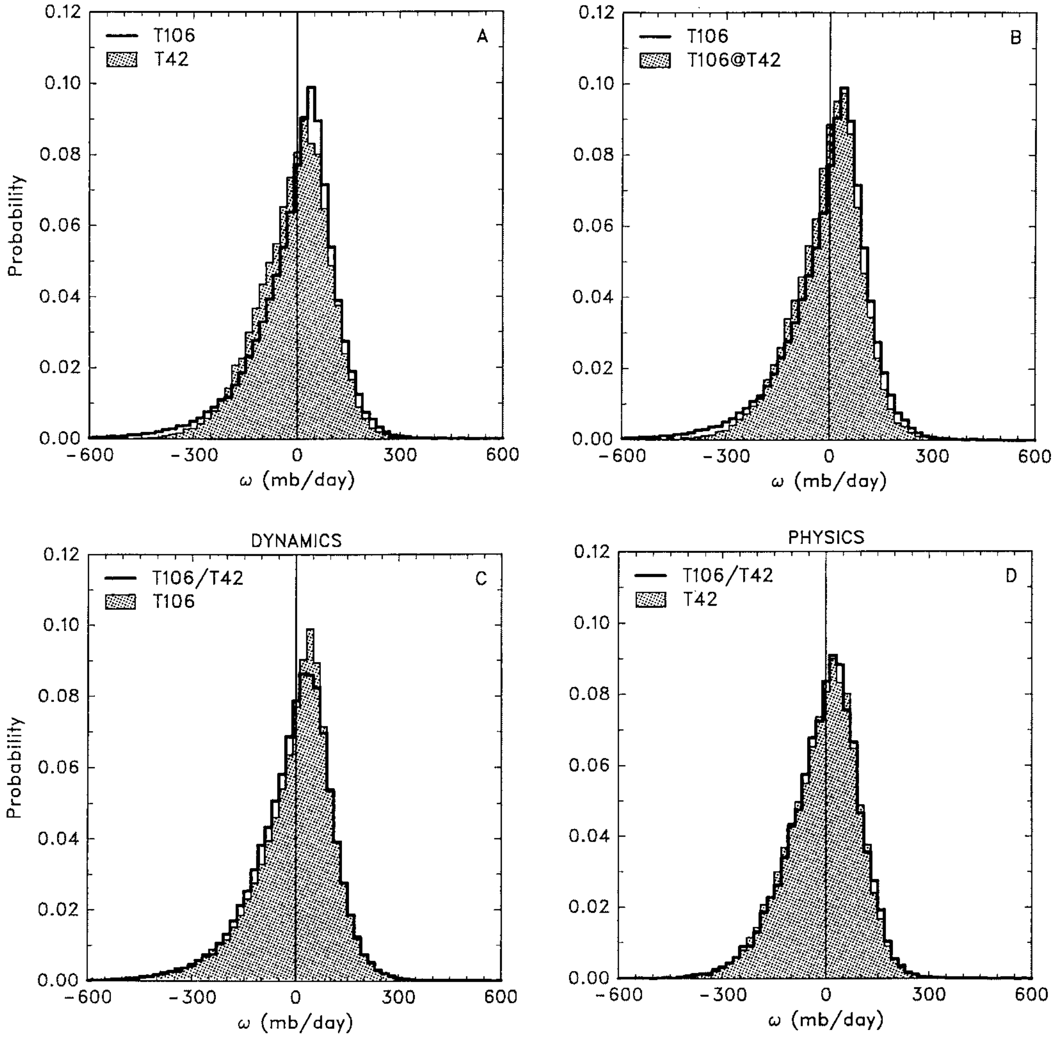

Fig. 3. January probability density distribution of ω at 850 mb in the North Atlantic storm track region (30°N to 60°N, 60°W to 30°W).

sumably most of it is associated with transient cyclones in the storm track rather than standing oscillations.

In addition to the strength of the vertical motion we examined the depth of the upward motion. We did this by asking: for a given reference level, if the vertical motion is upward, what is the fraction of the time it is upward at every level between that reference level and the level of interest, but is not upward at the level above that level of interest? Fig. 4A shows that probability density distribution for the North Atlantic storm track region for the T42 and T106 standard model simulations. The reference level is the 925 mb model level. (Although we label the distribution in terms of pressure, the calculation is based on model hybrid grid levels. The ordinate is the nominal pressure of the grid level based on 1000 mb surface pressure. The grid points are at the centers of the straight line segments of the plot. Note also, that the ordinate is linear in pressure, not in grid point level index so the visual integral of the distribution

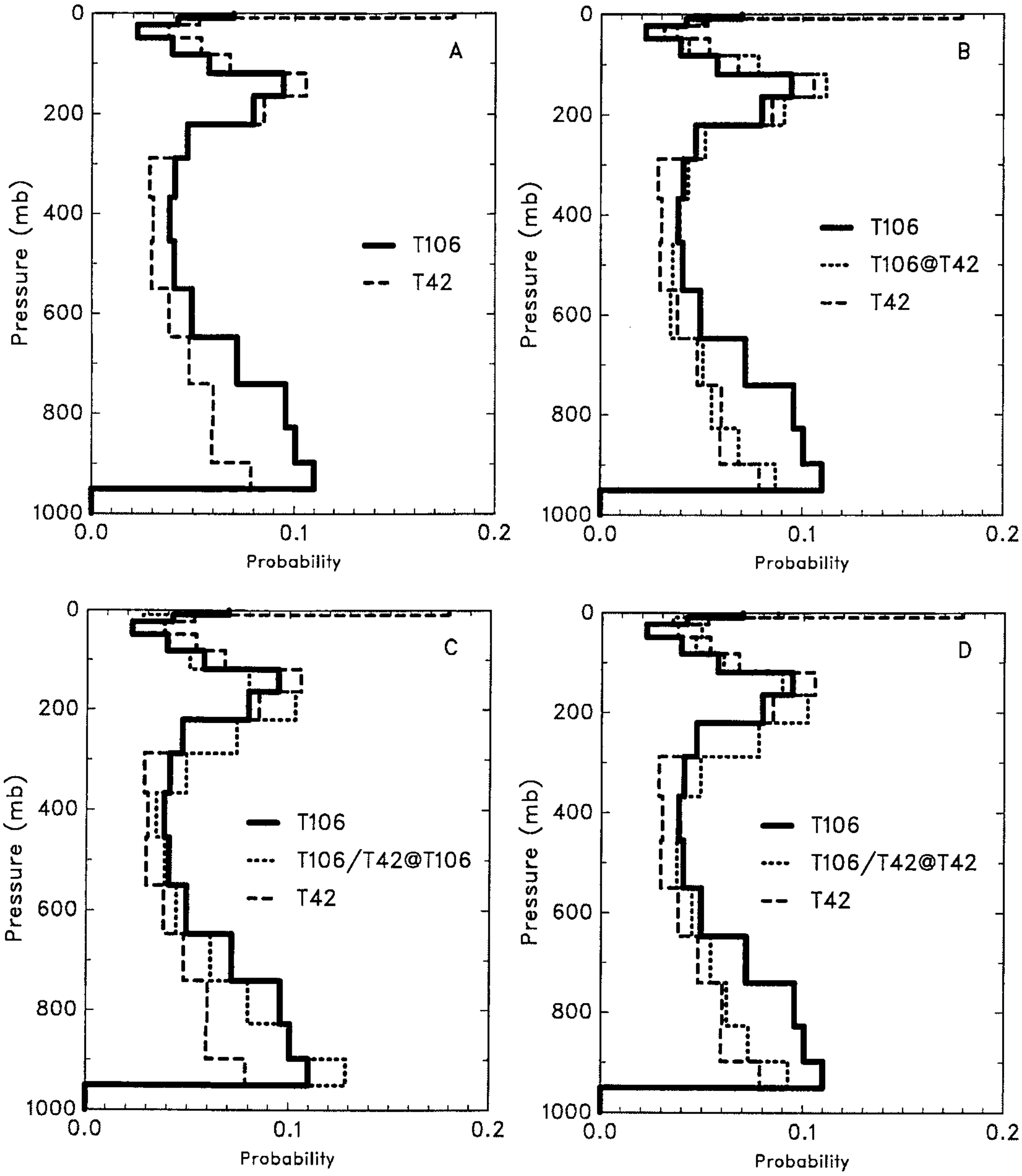

Fig. 4. January probability in the North Atlantic storm track region (30°N to 60°N, 60°W to 30°W) that if the vertical motion is upward at 925 mb, it is upward at every level between 925 and the level plotted, but not at the next level above.

(over pressure) from the plot will not appear to be the same as the distribution changes.) There is a distinct shift between the two resolutions. The T106 tends to have shallower cells of continuous upward motion. The T42 more often has upward vertical motion throughout the troposphere, through the tropopause and into the stratosphere. In fact, it has upward vertical motion continually up to the model top a relatively large fraction of the time.

Fig. 4B shows the distribution of daily ω from the standard T106 simulation truncated to T42 (labeled T106@T42) along with the those from the T106 and T42 standard model simulations. As before, the distribution of the truncated data matches the T42 simulation rather than the T106. (The value at the top model level for T106@T42 which is hidden by the T42 curve is 0.13.) Although overall the simulation is not converging, the large scale T42 component is. Fig. 4C shows the distribution from the T106 dynamical component of the dual-resolution T106/T42 simulation (labeled T106/T42@T106) compared to the T106 and T42 standard model distributions. (The value at the top model level for T106/T42@T106 which is hidden by the T106 curve is 0.05.) Fig. 4D shows the distribution from the T42 parameterization component of the dual-resolution T106/T42 simulation compared to the T106 and T42 standard model distributions. (The value at the top model level for T106/T42@T42 which is hidden by the T42 curve is 0.09.) We have also examined the distributions based on 970 and 850 mb reference levels and they are very similar to those in Fig. 4. Again, the T106 dynamical component in the dual-resolution model captures much of the T106 standard model simulation signal. The smaller scales of ω are not forced directly by the finer resolution parameterizations, but rather arise from nonlinear interactions in the dynamics. The truncated T42 component of the dual-resolution T106/T42 model seen by the parameterizations is closer to that of the standard T42 simulation.

We have also examined the characteristics of the vertical motion in the North Pacific storm track region. The characteristics are the same as those illustrated above for the Atlantic.

6. Conclusions

The characteristics of the convergence of the dual-resolution simulations with increasing horizontal dynamical resolution when the scale of the parameterizations is held fixed are very different for mid-latitude transient flow and tropical mean flow. The convergence in mid-latitudes was examined by considering the probability density distribution of pressure vertical velocity ω in the storm track regions. In simulations with both the standard and dual-resolution models there is a distinct shift in skewness toward subsidence with increasing horizontal resolution. In addition, the probability of stronger upward motion increases with higher resolution, while that of weaker upward motion decreases. These mid-latitude transient aspects do not converge when the scale of the physics is held fixed. The nonlinear interactions in the dynamics create finer scales, with or without the finer scale forcing. However, the lower resolution T42 scales themselves do converge, at least the aspects considered here, namely the storm track vertical motion probability density distribution. These convergence characteristics are shared with the standard model when its horizontal resolution is increased.

The local tropical Hadley circulation, on the other hand, does converge with increasing dynamical resolution when the scale of the physics is held fixed. The convergent state is close to that produced by the standard model at a resolution supported by the parameterization grid. In contrast, the standard model does not converge with increasing horizontal resolution up to at least T170, nor does the lower resolution T42 subset of the simulations converge. The lack of convergence seen in the full model is attributable to the direct forcing from the smaller scales included in the parameterization. The differences in ω are accompanied by differences in the physical parameterizations. For example, as resolution increases, condensation increases throughout the column of the ascending branch, where stronger ascending motion is producing more vertical transport by the resolved scales. This, of course, results in stronger heating from the release of latent heat, forcing stronger resolved upward motion.

These results raise a serious question — are the parameterizations correctly formulated in the model? If the parameterizations are accounting for the subgrid scale effects on the retained scales, then at T42 in the dual-resolution model they should provide the forcing of those scales that is explicitly calculated in the scales from T42 to T106 in the T106 standard model simulation. That appears not to be the case here. The parameterized forcing must be wrong in at least one of the two simulations. The parameterizations should explicitly take into account the scale of the grid on which it is applied. That does not seem to be common in parameterizations for global climate models today, although Chen and Bougeault (1993) have modified their convection parameterization with a resolution-dependent factor. Unfortunately, this adds another disposable parameter which must be determined; yet critical observations are unavailable for determining it, and it must be chosen based on characteristics of the simulations themselves at different resolutions.

7. Acknowledgments

I would like to thank John Truesdale for developing the code for these dual-resolution simulations and for running the experiments.

REFERENCES

Boyle, J. S. 1993. Sensitivity of dynamical quantities to horizontal resolution for a climate simulation using the ECMWF (Cycle 33) model. *J. Climate* **6**, 796–815.

Briegleb, B. P. 1992. Delta–Eddington approximation for solar radiation in the NCAR Community Climate Model. *J. Geophys. Res.* **97**, 7603–7612.

Chen, D. and Bougeault, P. 1993. A simple prognostic closure assumption to deep convective parameterization: Part I. *Acta. Meteorologica Sinica* **7**, 1–18.

Déqué, M., Dreveton, C., Braun, A. and Cariolle, D. 1994. The ARPEGE/IFS atmosphere model: a contribution to the French community climate modelling. *Clim. Dynamics* **10**, 249–266.

Déqué, M. and Piedelievre, J. Ph. 1995. High resolution climate simulation over Europe. *Clim. Dynamics* **11**, 321–339.

Hack, J. J. 1994. Parameterization of moist convection in the National Center for Atmospheric Research Community Climate Model (CCM2). *J. Geophys. Res.* **99**, 5551–5568.

Hack, J. J., Boville, B. A.,Briegleb, B. P., Kiehl, J. T., Rasch, P. J. and Williamson, D. L. 1993. *Description of the NCAR Community Climate Model (CCM2).* NCAR Technical Note NCAR/TN-382+STR, 108 pp.

Hack, J. J., Boville, B. A., Kiehl, J. T., Rasch, P. J. and Williamson, D. L. 1994. Climate statistics from the NCAR Community Climate Model (CCM2). *J. Geophys. Res.* **99**, 20785–20813.

Holtslag, A. A. M. and Boville, B. A. 1993. Local versus nonlocal boundary-layer diffusion in a global climate model, *J. Climate* **6**, 1825–1842.

Kiehl, J. T. and Briegleb, B. P. 1991. A new parameterization of the absorptance due to the 15 μm band system of carbon dioxide. *J. Geophys. Res.* **96**, 9013–9019.

Kiehl, J. T. and Williamson, D. L. 1991. Dependence of cloud amount on horizontal resolution in the NCAR Community Climate Model. *J. Geophys. Res.* **96**, 10,955–10,980.

Kiehl, J. T., Hack, J. J. and Briegleb, B. P. 1994. The simulated earth radiation budget of the National Center for Atmospheric Research CCM2 and comparisons with the Earth Radiation Budget Experiment (ERBE). *J. Geophys. Res.* **99**, 20,815–20,827.

McFarlane, N. A. 1987. The effect of orographically excited wave drag on the general circulation of the lower stratosphere and troposphere. *J. Atmos. Sci.* **44**, 1775–1800.

Potter, G. L. 1995. *The effect of horizontal resolution on cloud radiative forcing in the ECMWF model.* PCMDI Report no. 22., Program for Climate Model Diagnosis and Intercomparison, Lawrence Livermore National Laboratory, Livermore, CA 94550, 28 pp.

Shea, D. J., Trenberth, K. E. and Reynolds, R. W. 1990. *A global monthly sea surface temperature climatology.* NCAR Technical Note NCAR/TN-345+STR, Boulder, Colorado, 167 pp.

Sperber, K. R., Hameed, S., Potter, G. L. and Boyle, J. S. 1994. Simulation of the northern summer monsoon in the ECMWF model: Sensitivity to horizontal resolution. *Mon. Wea. Res.* **122**, 2461–2481.

Stratton, R. A. 1999. A high resolution AMIP integration using the Hadley Centre model HadAM2b. *Clim. Dynamics* **14**, 9–28.

Stephenson, D. B. and Royer, J.-F. 1995. GCM simulation of the Southern Oscillation from 1979–88. *Clim. Dynamics* **11**, 115–128.

Stephenson, D. B., Chauvin, F. and Royer, J.-F. 1998. Simulation of the Asian summer monsoon and its dependence on model horizontal resolution. *J. Meteor. Soc. Japan* **76**, 237–265.

Williamson, D. L. and Rasch, P. J. 1994. Water vapor transport in the NCAR CCM2. *Tellus* **46A**, 34–51.

Williamson, D. L., Hack, J. J. and Kiehl, J. T. 1995. Climate sensitivity of the NCAR Community Climate Model (CCM2) to horizontal resolution. *Clim. Dynamics* **11**, 377–397.